ELSEVIER

Available online at www.sciencedirect.com
SCIENCE DIRECT®

Journal of Crystal Growth 272 (2004) 538–542

JOURNAL OF CRYSTAL GROWTH

www.elsevier.com/locate/jcrysgro

MOCVD growth of highly strained InGaAs:Sb–GaAs–GaAsP quantum well vertical cavity surface-emitting lasers with 1.27 μm emission

H.C. Kuo[a,*], H.H. Yao[a], Y.H. Chang[a], Y.A. Chang[a], M.Y. Tsai[a], J. Hsieh[b], E.Y. Chang[b], S.C. Wang[a]

[a]*Institute of Electro-optical Engineering, National Chiao-Tung University, 1001 Ta-Hsieh Rd, Hsin-Tsu, Taiwan, ROC*
[b]*Department of Material Engineering, National Chiao-Tung University, 1001 Ta-Hsieh Rd, Hsin-Tsu, Taiwan, ROC*

Available online 12 October 2004

Abstract

1.27 μm InGaAs:Sb–GaAs–GaAsP vertical cavity surface-emitting lasers (VCSELs) were grown by metalorganic chemical vapor deposition (MOCVD) with superior performance. The threshold current changes between 1.8 and 1.1 mA and the slope efficiency drops below ~35% when the temperature is raised from room temperature to 70 °C. With only 5 mA of bias current, the 3 dB modulation frequency response is measured to be 8.36 GHz which is suitable for 10 Gb/s operation. The maximal bandwidth is estimated to 10.7GHz with modulation current efficiency factor (MCEF) of $\sim 5.25\,\mathrm{GHz/(mA)^{1/2}}$. The results of InGaAs:Sb–GaAs–GaAsP VCSELs can reach a performance level comparable to GaInAsN VCSELs with better thermal stability and should be considered as a very promising candidate for 1.3 μm commercial applications.
© 2004 Elsevier B.V. All rights reserved.

PACS: 81.15.G; 85.60.J; 68.55.J

Keywords: A3. Metalorganic chemical vapor deposition; B1. Antimonides; B2. Semiconducting indium compounds; B3. Optical fiber devices; B3. Vertical cavity surface emitting laser

I. Introduction

Long-wavelength vertical cavity surface-emitting lasers (VCSELs) are key devices in the optical fiber metropolitan-area networks (MAN) [1]. To date, the most promising results on low-cost long-wavelength lasers or VCSELs have been obtained using GaInAsN quantum wells (QWs) grown on GaAs substrates [1–5]. The large conduction band offset leads to the improvement of temperature performance compared to conventional InP-based materials, and the GaAs system provides

*Corresponding author. Tel.: +886 3 571 2121; fax: +886 3 571 6631.
E-mail address: hckuo@faculty.nctu.edu.tw (H.C. Kuo).

0022-0248/$ - see front matter © 2004 Elsevier B.V. All rights reserved.
doi:10.1016/j.jcrysgro.2004.08.092

high-performance AlGaAs/GaAs DBR mirrors and allows the use of well-established oxide-confined GaAs-based VCSEL manufacturing infrastructure. However, GaInAsN is a very challenging materials system from a growth point of view: (1) it is difficult to incorporate N into the InGaAs QW and the introduction of N into QW increases the non-radiative (monomolecular and Auger) recombination and thus lowers the material gain and increases transparent carrier density [6]; (2) During post-growth annealing, the anneal nitrogen diffuses out from the quantum well and blue-shifts optical emission. Recently, highly strained InGaAs VCSELs with photoluminescence (PL) peak at 1.205 μm and laser emission wavelength ~1.26–1.27 μm demonstrated very promising performance and continuous-wave (CW) operation up to 120 °C as well as 10 Gb/s operation [7]. However, the emission wavelength of 1.26 μm is barely in compliance with optical communication standards such as IEEE 820.3ae 10 Gb/s Ethernet. In addition, the laser has a relatively poor performance at room temperature due to the large negative gain-cavity offset. Antimony (Sb) present during GaInAsN growth has been thought to act as a surfactant and improve PL [8]. The authors have observed that adding Sb to samples with high Indium content sharply increases the intensity, and have found that the alloy thus formed not only behaves as a surfactant but contributes significantly red-shifting the optical emission [8]. Additionally, the critical layer thickness for InGaAs on GaAs can be significantly increased with the additional surfactant such as Sb [9] and Te [10]. In this paper, we present the high-performance InGaAs:Sb–GaAs–GaAsP QW VCSELs grown by metal organic chemical vapor deposition (MOCVD). These VCSELs exhibit superior performance and temperature stability. The threshold current changes between 1.8 and 1.1 mA and the slope efficiency drops less than ~35% when the temperature is raised from room temperature to 70 °C. With only 5 mA of bias current, the 3 dB modulation frequency response is measured to be 8.36 GHz which is suitable for 10 Gb/s operation. The maximal bandwidth is estimated to be 10.7 GHz with MCEF of ~5.25 GHz/(mA)$^{1/2}$.

2. Experimental details

All structures were grown on Semi-insulating GaAs (1 0 0) substrates by low pressure (60 Torr) MOCVD. Group-V precursors are the hydride sources AsH_3 and PH_3. The trimethyl alkyls of gallium (Ga), aluminum (Al), indium (In) and Antimony (Sb) are the group-III precursors. The epitaxial structure is as following (from bottom to top): an n^+-GaAs buffer, a 40.5-pair n^+-$Al_{0.9}Ga_{0.1}As$/n^+-GaAs (Si-doped) distributed Bragg reflector (DBR), undoped active region, a p-$Al_{0.98}Ga_{0.02}As$ oxidation layer, a 25-pair p^+-$Al_{0.9}Ga_{0.1}As$/p^+-GaAs DBR (carbon-doped), and a p^+-GaAs (carbon-doped) contact layer. The graded-index separate confinement heterostructure (GRINSCH) active region mainly consists of a double QW active region $In_{0.41}Ga_{0.59}As$:Sb–GaAs–$GaAs_{0.85}P_{0.15}$ (60 Å/100 Å/100 Å) with a PL emission at 1.214 μm embedded between two linear-graded $Al_xGa_{1-x}As$ ($x = 0$–0.6 and $x = 0.6$–0) confinement layers (growth temperature = 550 °C with AsH_3/III ratio as low as 20 and Sb/V ratio 0.005). The optical pyrometer was used to measure the substrate temperature between 400 and 800 °C. The pyrometer was calibrated to the melting point of InSb. The thickness of the cavity active region is 1λ. Carbon was used as the p-type dopant in the DBR to obtain higher carrier concentration (2–$3 \times 10^{18}\,cm^{-3}$). The interfaces of both the p-type and n-type $Al_{0.9}Ga_{0.1}As$/GaAs DBR layers are linearly graded to reduce the series resistance. The growth rate is ~1 μm/h for InGaAs:Sb QW region and ~2 μm/h for $Al_{0.9}Ga_{0.1}As$/GaAs DBR region. The optical properties of QWs were optimized through PL measurement and structural analysis is described as follows. The FP-dip wavelength is at 1270 nm, which was determined by reflection measurement.

To optimize growth parameters, we need to investigate critical layer thickness (CLT) of InGaAs grown on GaAs with the effect of Sb surfactant. In lattice-mismatched systems, the strain of the layers is accommodated elastically in layers thinner than a misfit-dependent critical thickness as described by Matthews and Blakeslee [11]. Fig. 1 shows the numerical calculation of the

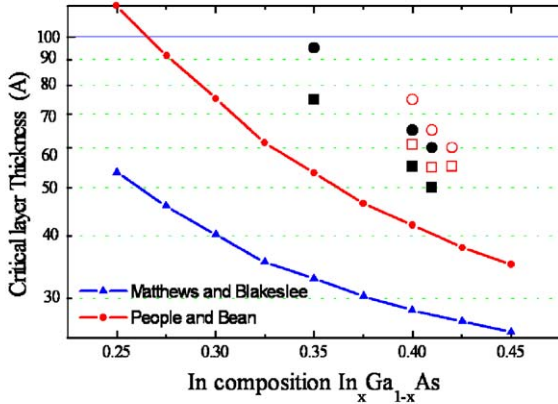

Fig. 1. Numerical calculation of the critical thickness for $In_xGa_{1-x}As$–GaAs as a function of indium composition x in the range $0.25<x<0.45$. Full symbols represent the QWs where their defects were not observed. Open symbols indicate that QWs show faceting or dislocations. Square symbols represent InGaAs grown on GaAs, while circle symbols represent InGaAs grown on GaAs with ~1.5% Sb incorporation.

critical thickness for $In_xGa_{1-x}As$–GaAs as a function of indium composition x in the range $0.25<x<0.45$. Substituting the critical thickness as a function of Indium composition for the width of the quantum well, the energy states are calculated for the first level in the QW. The maximal wavelength that can be achieved is less than 1100 nm. However, a recent publication demonstrated that the critical thickness of InGaAs on GaAs is larger than Matthews and Blakeslee's predication and the maximal wavelength that can be achieved is ~1200 nm [12,13]. People and Bean have proposed an alternative description for the critical thickness by defining a balance between the strain energy in an epitaxial layer and the formation energy of an isolated screw dislocation [14]. This critical thickness is also plotted in Fig. 1, and can be increased using this model. Additionally, the critical thickness of InGaAs on GaAs can be enhanced by additional strain compensating layer or surfactant [9]. TEM measurements were used to determine the formation of faceting or dislocations. Full symbols represent the QWs where the defects were not observed. Open symbols indicate that QWs show faceting or dislocations. Square symbols represent InGaAs

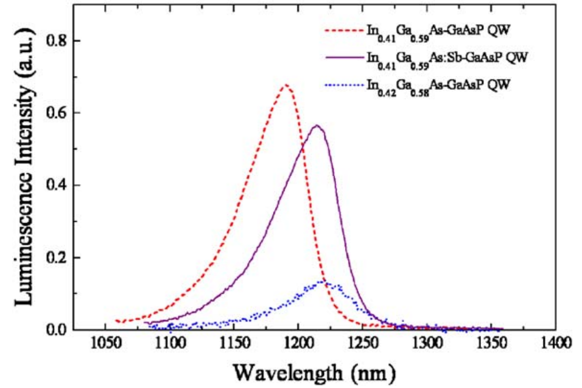

Fig. 2. Comparison of the photoluminescence spectra of InGaAs with different In composition and $In_{0.41}Ga_{0.59}As$ with Sb incorporation.

grown on GaAs, while circle symbols represent InGaAs grown on GaAs with ~1.5% Sb incorporation (measured by SIMS). It is clear that with Sb incorporation, the CLT of InGaAs on GaAs increases. No dislocations were observed for 75 Å $In_{0.4}Ga_{0.6}As$:Sb/GaAs, 60 Å $In_{0.41}Ga_{0.59}As$:Sb/GaAs and 50 Å $In_{0.42}Ga_{0.58}As$:Sb/GaAs QWs. These results are consistent with the observations of Ref. [9].

Fig. 2 shows the comparison of the photoluminescence spectra of $In_xGa_{1-x}As$ QWs with different In composition ($x=0.41$ and 0.42) and $In_{0.41}Ga_{0.59}As$ QW with Sb incorporation. All samples have well thickness of 60 Å with GaAs spacer and $GaAs_{0.85}P_{0.15}$ strain compensating layer. The PL peak emission wavelengths (λ_p) of the grown $In_{0.41}Ga_{0.59}As$/GaAs/GaAsP and $In_{0.41}Ga_{0.59}As$:Sb/GaAs/GaAsP QWs are 1.194 and 1.214 μm, respectively. A red shift of 20 nm is observed. For $In_{0.41}Ga_{0.59}As$:Sb, the full-width at half-maximum (FWHM) of the PL emission peak is larger and PL intensity is slightly lower. More Indium incorporation or the lower of conduction band lineup can also explain the red-shift of the optical emission. As the In composition increases to 0.42, the FWHM of PL emission increases drastically and the PL intensity drops significantly. This can be explained by the dislocations as well as non-radiative defects formation in 60 Å $In_{0.42}Ga_{0.58}As$/GaAs/GaAsP QW (60 Å is larger than the CLT).

3. Device results

The schematic VCSEL structure can be shown in Fig. 3. A processing sequence included six photomasks to fabricate oxide-confined polyimide-planarized VCSELs with coplanar waveguide probe pads. This process was designed to minimize capacitance while keeping reasonably low resistance [15]. Device fabrication began with the formation of cylindrical mesas with a diameter of 30 μm by etching the surrounding semiconductor into the bottom n-type mirror to a depth of 5 μm, using an ICP–RIE system. The sample was wet-oxidized in a 420 °C steam environment for 20 min to form the current aperture and provide lateral index guiding to the lasing mode. The oxidation rate was 0.6 μm/min for the $Al_{0.98}Ga_{0.02}As$ layer, so the oxide extended 12.5 μm from the mesa sidewall. Ti/Au was evaporated to form the p-type contact ring, and AuGeNiAu was evaporated onto the etched n-buffer layer and etched bottom mirror to form the p-type contact, which is connected to the semi-insulating substrate. Contacts were alloyed for 30 s at 420 °C using RTA. After the contact formation, the photosensitive polyimide was spun on the sample to form insulation and planarization. Ti–Au was deposited to a thickness from 200–3000 Å to form the metal interconnects and coplanar waveguide probe pads. Heat treatment following metal deposition was applied to strengthen the metal-to-polyimide adhesion. Finally, surface relief etching with a diameter of 3.5 μm was performed to a depth of ~100 nm to support single-mode operation [16].

The DC characteristics of completed VCSELs were measured using a probe station, an Agilent 4145 A semiconductor parameter analyzer and an InGaAs photodiode. The spectra of the InGaAs:Sb–GaAs–GaAsP VCSELs were measured using an Advantest Q8381 A optical spectrum analyzer. Fig. 4 plots curves of temperature-dependent light output and voltage versus current (LIV). The devices exhibit single transverse mode characteristics at a lasing wavelength of ~1.27 μm, with a side mode suppression ratio (SMSR) of >30 dB as shown in the inset in Fig. 4 over the whole operating range. Notably, the maximal single mode output power exceeds 1.2 MW at room temperature (0.8 MW at 70 °C). Output power rollover occurs as the current increases above 10 mA at 25 °C (9.5 mA at 70 °C). The threshold current changes between 1.8 and 1.1 mA with temperatures between 25 and 70 °C and the drop of slope efficiency is less than ~35% from 0.17–0.11 MW/mA due to the large gain-cavity offset. The resistance of the VCSEL is ~120 Ω and the capacitance is ~0.1 pF. Accordingly, parasitic effects limit the devices to a frequency response of around 13 GHz.

The small signal response of VCSELs as a function of bias current was measured using a calibrated vector network analyzer (Agilent 8720) with on-wafer probing and a 50 μm multimode optical fiber connected to a New Focus 25 GHz photodetector. Fig. 5 shows that the modulation frequency increases with the bias current, until it

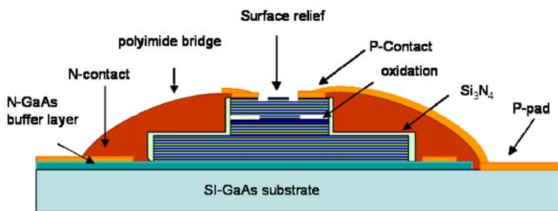

Fig. 3. Schematic cross section of high-speed VCSEL structure. The oxide-confined aperture is 5 μm and the surface relief size is 3.5 μm.

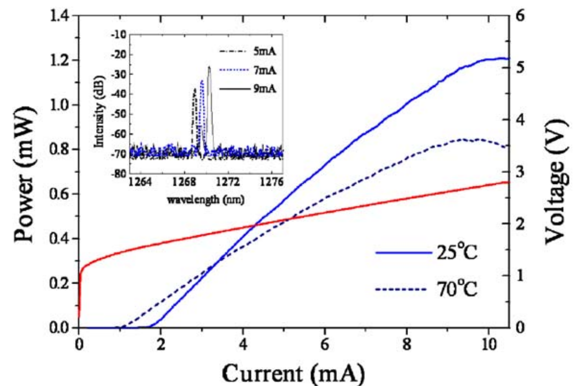

Fig. 4. Temperature-dependent light output and voltage versus current (LIV) curves. Inset is the emission spectra of InGaAs:Sb–GaAs–GaAsP VCSELs at different driving currents.

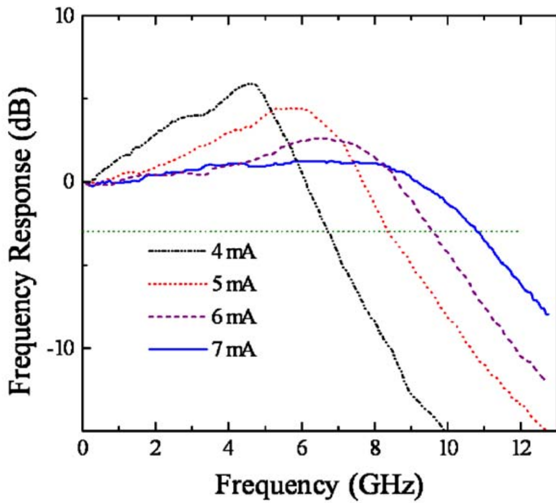

Fig. 5. High-speed modulation measurement on VCSELs. The maximal bandwidth is estimated to be 10.7 GHz with MCEF of ~5.25 GHz/(mA)$^{1/2}$.

flattens at a bias of about 7 mA. At a bias current of only 5 mA, a maximum 3dB frequency is measured as 8.36 GHz, which is suitable for 10 Gb/s operation. The maximal bandwidth is estimated to be 10.7 GHz with MCEF of ~ 5.25 GHz/(mA)$^{1/2}$.

4. Conclusion

High-performance InGaAs:Sb–GaAs–GaAsP QWs VCSELs were successfully grown by MOCVD. These VCSELs show very low threshold current, good temperature performance, and high-modulation bandwidth ~ 10.7 GHz with MCEF of ~5.25 GHz/(mA)$^{1/2}$. The results of InGaAs:Sb VCSELs can reach a performance level comparable to GaInAsN VCSELs with better thermal stability and should be considered as a very promising candidate for 1.3 μm commercial applications.

Acknowledgements

The authors would like to thank Dr. Chihping Kuo of LuxNet Corporation, Drs. C. P. Sung and Jim Chi of ITRI and Prof. Nelson Tansu of Lehigh University for useful discussion and technical support. This work was partially supported by the National Science Council of the Republic of China (ROC) in Taiwan under Contract no. NSC 90-2215-E-009-102 and by the Academic Excellence Program of the ROC Ministry of Education under Contract no. 88-FA06-AB. The support by the Institute of Nuclear Energy under Contract no. 922001InER015 of the proton implantation is also gratefully acknowledged.

References

[1] M. Tan, Progress in long wavelength VCSELs, Lasers and Electro-Optics Society, 2002. The 15th Annual Meeting of the IEEE, vol. 1, 2002, pp. 269–270.

[2] M. Kondow, T. Kitatani, S. Nakatsuka, M.C. Larson, K. Nakahara, Y. Yazawa, M. Okai, K. Uomi, IEEE J. Select. Topic Quantum Electron. 3 (1997) 719–730.

[3] K.D. Choquette, J.F. Klem, A.J. Fischer, O. Blum, A.A. Allerman, I.J. Fritz, S.R. Kurtz, W.G. Breiland, R. Sieg, K.M. Geib, J.W. Scott, R.L. Naone, Electron. Lett. 36 (16) (2000) 1388–1390.

[4] T. Takeuchi, Y.-L. Chang, M. Leary, A. Tandon, H.-C. Luan, D. Bour, S. Corzine, R. Twist, M. Tan, Electron. Lett. 38 (2002) 1438–1440.

[5] M. Kawaguchi, T. Miyamoto, E. Gouardes, D. Schlenker, T. Kondo, F. Koyama, K. Iga, Jpn. J. Appl. Phys. 40 (2001) L744–L746.

[6] N. Tansu, L.J. Mawst, IEEE Photon. Technol. Lett. 14 (2002) 1052–1054.

[7] P. Sundgren, R.M. von Wurtemberg, J. Berggren, M. Hammar, M. Ghisoni, V. Oscarsson, E. Odling, J. Malmquist, Electron. Lett. 39 (2003) 1128–1129.

[8] V. Gambin, Ha Wonill, M. Wistey, Yuen Homan, S.R. Bank, S.M. Kim, J.S. Harris, IEEE J. Select. Topic Quantum Electron. 8 (2002) 795–800.

[9] J.C. Harmand, L.H. Li, G. Patriarche, L. Travers, Appl. Phys. Lett. 84 (2004) 3981–3983.

[10] J. Massies, N. Grandjean, V.H. Etgens, Appl. Phys. Lett. 61 (1992) 99–101.

[11] J.W. Matthews, A.E. Blakeslee, J. Crystal Growth 27 (1974) 118.

[12] N. Tansu, J.Y. Yeh, L.J. Mawst, Appl. Phys. Lett. 82 (23) (2003) 4038–4040.

[13] N. Tansu, Y.L. Chang, T. Takeuchi, D.P. Bour, S.W. Corzine, M.R.T. Tan, L.J. Mawst, IEEE J. Quantum Electron. 38 (6) (2002) 640–651.

[14] R. People, J.C. Bean, Appl. Phys. Lett. 47 (1985) 322.

[15] H.C. Kuo, Y.S. Chang, F.Y. Lai, T.H. Hsueh, L.H. Laih, S.C. Wang, Electron. Lett. 39 (14) (2003) 1051–1053.

[16] J. Heiko Unold, W.Z. Safwat, R. Mahmoud Jäger, M. Grabherr, R. Michalzik, K.J. Ebeling, IEEE J. Select. Topics Quantum Electron. 7 (2000) 386–392.